Published May 23, 2019

Original Research

Core Ideas

- Green roofs comprise a soilless medium over an atmospheric equilibrated space.
- Green roofs represent microcosms of capillary fringe and vadose zone hydraulics.
- Bulk properties come from the interparticle voids and the intraparticle pores.
- Capillary retention is fundamental for water storage in a green roof system.
- Design specifications for green roofs should focus on using a well-graded medium.

The Effect of Intraparticle Porosity and Interparticle Voids on the Hydraulic Properties of Soilless Media

Jenny Hill,* Brent Sleep, Jennifer Drake, and Marisa Fryer

An essential component of a building-integrated vegetation system, such as an extensive green roof, is the layer of lightweight planting medium that supports rooting and stores water. Predicting and describing the stormwater management performance of green roofs requires reliable data regarding the water retention properties of the planting medium. Ten materials proposed for use on green roofs, including four mineral components, three biological components, and three commercial blends, were characterized through measurement of their water release curves (WRCs). In combination with the particle size distributions, the resultant data demonstrate that some of the materials contain measurable intraparticle pore networks in addition to the interparticle void spaces described in classical soil hydrology. The WRCs were also used to model the maximum water storage under static equilibrium conditions throughout a 15-cm profile of each material. In freely draining, unsaturated green roof systems, the role of the intraparticle pores may be limited to increasing microscale roughness of particle surfaces, thereby reducing film flow under drier conditions. The highly organic, biologically derived materials—screened compost, bark fines, and shredded wood—demonstrated hydrophobicity when air dried, but wetting occurred within <30 min on all occasions, which would be within the time frame of many rainstorms. As with natural soils, the saturated hydraulic conductivity was lower in materials with a higher proportion of fines (<106 μm).

Abbreviations: FAS, free air space; LEA, lightweight expanded aggregate; OM, organic matter; PAW_{15}, plant available water at 15 cm head; PSD, particle size distribution; WRC, water release curve.

J. Hill, Sustainable Technologies, Toronto and Region Conservation Authority, 5 Shoreham Drive, Toronto, ON L4K 5R6, Canada; B. Sleep, J. Drake, and M. Fryer, Dep. of Civil and Mineral Engineering, Univ. of Toronto, 35 St. George Street, Toronto, ON M5S 1A4, Canada. *Corresponding author (jenny.hill@trca.on.ca).

Received 17 Sept. 2018.
Accepted 29 Jan. 2019.

Citation: Hill, J., B. Sleep, J. Drake, and M. Fryer. 2019. The effect of intraparticle porosity and interparticle voids on the hydraulic properties of soilless media. Vadose Zone J. 18:180176. doi:10.2136/vzj2018.09.0176

Extensive green roofs are designed and installed in new and retrofit scenarios to provide a wide array of benefits to their host building and at an infrastructural scale across urban environments (Yocca and Sale, 2012). One such benefit is the retention of stormwater. Green roofs help reduce peak storm flows and volumes discharged to storm and combined sewer systems (Nawaz et al., 2015). On an annual basis, extensive green roofs can capture, store, and evapotranspire 40 to 70% of the total precipitation (Fassman-Beck et al., 2016; Hill et al., 2017). Extensive green roofs comprise a layer of lightweight, typically soilless, planting medium, to a maximum depth of 15 cm, that is used to support the growth of plants (Czemiel Berndtsson, 2010). As green roofs become increasingly popular as a means of stormwater management, many planting medium materials are being been trialed and/or modeled to provide information for water resources engineers and designers.

To reduce loading on building roof structures, most extensive green roof media comprise a mixture of coarse-textured, soilless, granular materials. Mineral-based examples include lightweight expanded shale or clay, crushed brick, and other recycled construction materials; biologically derived examples include chipped bark, wood mulch, and composted wood products. In the European market, mixtures usually contain a small fraction of biological material, in concordance with the guidelines of Forschungsgesellschaft Landschaftsentwicklung–Landschaftsbau (2008), whereas in some North American regions, soilless mixtures containing a much higher proportion of organic matter (OM) are being used (Hill et al., 2016). The organic content is frequently needed to provide nutrients to support plant growth, and the biological material is typically lighter weight (Sandoval et al., 2017). However, the use of large quantities of biological material in green roof media

has been associated with the leaching of excess nutrients in runoff water (Czemiel Berndtsson, 2010; Van Seters et al., 2009), and these media have been observed to shrink (Schindler et al., 2016) and become hydrophobic (Raviv et al., 2008b) when dried.

Research regarding the retention of stormwater in extensive green roof media has considered a great many materials and combinations. These most often include some form of naturally porous mineral with added biological materials (Burszta-Adamiak, 2012; Ma et al., 2012; Schroll et al., 2011; Uhl and Schiedt, 2008; Voyde et al., 2010) and/or man-made expanded aggregates with added biological materials (Carter and Rasmussen, 2006; Cronk, 2012; Gregoire and Clausen, 2011; Hathaway et al., 2008; Prowell, 2006; VanWoert et al., 2005). Biologically derived materials with high OM content are usually incorporated in small quantities, and then the bulk properties are assessed (Molineux et al., 2009).

In natural soils, the particle size distribution (PSD) is often used to predict a soil's maximum water capacity (Nelson and Rittenour, 2015; Wang et al., 2008) and saturated hydraulic conductivity (K_{sat}) (Chapuis, 2012; Salarashayeri and Siosemarde, 2012) through statistical processes termed *pedotransfer functions* (Pachepsky and Rawls, 2004; van Genuchten et al., 1991). These relationships are usually derived from empirical evidence. The physical principles that determine water behavior are based on two related assumptions: (i) the porous medium is comprised of regularly shaped, inert particles and (ii) the pore size distribution can be inferred from the PSD. The PSD of the relatively coarse green roof planting media is readily measured through sieving (Carbone et al., 2014; Poë et al., 2011; Yuristy, 2013). However, for green roof media, which often comprise a high proportion of materials with internal porosity, such as expanded aggregates or compost, it may be erroneous to infer the pore size distribution from the more readily measured PSD owing to the unusual physical properties of the constituent particles (Liu and Fassman-Beck, 2017).

Because green roof materials often have high organic content, it is important to consider that materials with high organic content can demonstrate hydrophobicity and shrink–swell characteristics, which affect bulk properties (Petrell and Gumulia, 2013). Hydraulic conductivity can vary with θ in biologically derived materials. For example, Khoshand and Fall (2014) reported a U-shaped relationship between the two parameters; a twofold decrease in the hydraulic conductivity of their compost occurred between θ = 0.2 and 0.4, which corresponded with the maximum dry density at θ = 0.4, and then an increase in hydraulic conductivity was observed between θ = 0.4 and 0.6 owing to higher connectivity of the wetted regions and a trend toward K_{sat}.

Total annual stormwater retention is constrained by the inherently limited capacity of the green roof and the distribution of storm depths (Adams and Papa, 2000). This means that a proportion of the received rainstorms will exceed the storage of the green roof system, producing discharge water or runoff (Stovin et al., 2015). For this reason, extensive green roofs also contain a drainage layer immediately beneath the planting medium, separated with a geotextile to maintain the free space beneath. This layer prevents ponded water from penetrating a leaky roof membrane and/or damaging the plant root system. Drainage layers are often preformed plastic but may be constructed with a coarse, freely draining aggregate layer (Forschungsgesellschaft Landschaftsentwicklung–Landschaftsbau, 2008; Optigrün International, 2008; Roofmeadow, 2013).

Because extensive green roofs are comprised of 10 to 15 cm of lightweight soilless media suspended over an atmospheric equilibrated void space (i.e., the drainage layer), they represent interesting microcosms of vadose zone hydraulics. Under the hottest, dry weather conditions, the media can reach much higher temperatures than the local ground conditions and become exceptionally dry. At the other extreme, even the deepest rainstorm events will not leave the profile any more saturated than a capillary fringe owing to the highly permeable geotextile at the lower boundary.

A green roof system at maximum water storage would cease to drain when hydrostatic equilibrium is reached (Fig. 1). Because the lower boundary is a seepage face, there will be complete saturation of the planting medium at the lower boundary with the geotextile (Handreck and Black, 2002; Iwata et al., 1994). A meniscus forms at every void along the geotextile, and matric potential becomes more negative upward through the profile, analogous to the capillary fringe in a subterranean environment. Then the maximum water storage of green roof system will depend on the slope and shape of the water release curve (WRC) of the medium, as indicated by the dashed line in Fig. 1.

Comparable conditions have been observed and described for potting containers at plant nurseries (Cassel and Neilsen, 1986; Handreck and Black, 2002; Heller et al., 2015) and for the maintenance of golf courses and sports fields (McCoy, 2014), but this hydraulic condition is not incorporated into most green roof models (Li and Babcock, 2014). Programs commonly used by design and engineering consultants, such as EPA-SWMM (Rossman and Huber, 2015), treat the water holding capacity of a green roof medium as a fixed property throughout the profile. Similarly, Kasmin et al. (2010) defined the water storage of a green roof as the product of medium depth and the maximum water holding capacity of the medium.

Zhang and Guo (2012) also used this type of linear relationship in their analytical probabilistic green roof model. Metselaar

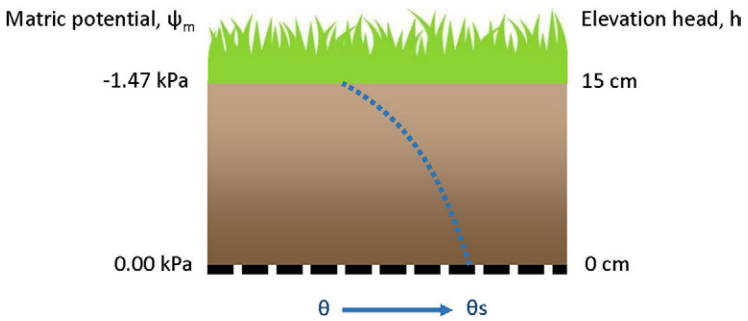

Fig. 1. Green roof matric potential (left) as a function of medium depth under static equilibrium with maximum water storage. θ, volumetric water content; θ_s, saturated volumetric water content.

(2012) used the Soil Water Atmosphere and Plant (SWAP) model to simulate the performance of four green roof planting media, including fine sand and peat moss, over 46 yr, using a seepage face boundary. The SWAP model demonstrated that, with this lower boundary condition, there is a nonlinear relationship between medium depth and the fraction of rainfall retained. The SWMS-2D model used by Palla et al. (2009) included a geotextile between the planting medium (Vulcaflor) and the underlying coarse drainage layer (lapillus). The vertical profile of water content during a simulated storm event illustrated that the hydraulic conductivity of the geotextile boundary was most influential in maintaining a horizontal wetting front. She and Pang (2010) instead reasoned that the wide range of pore sizes found in their planting medium meant that gravity drainage would occur from their green roof system through the network of macropores before saturation was reached.

This study presents the physical properties of the interparticle void spaces and the intraparticle pores found within common soilless granular materials and assesses their influence on the bulk hydraulic properties of the green roof systems as suspended vadose zone environments. The distribution of water within the green roof profile has implications both for stormwater capture (Carter and Jackson, 2007; Hilten et al., 2008; Qin et al., 2012; Uhl and Schiedt, 2008) and for the healthy growth of the plants (Breuning, 2013; MacIvor et al., 2013; Rowe et al., 2014). Green roof plantings are essential in maintaining stakeholder engagement with the system (McGlade and Hill, 2014) and in preventing wind scour and associated media loss (Hill et al., 2015). Within the growing media, higher plant available water storage is essential to keep a plant's tissues turgid and growing, and a free air space (FAS) of ≥10% is recommended in the rooting zone to prevent waterlogging and rotting (Raviv et al., 2008a).

There have been many laboratory studies describing the hydraulics of planting media for green roof applications (Babilis and Londra, 2011; Dal Ferro et al., 2014; Poë et al., 2015; Sandoval et al., 2017). Although these studies have focused on particle size and interparticle pore spaces, there remains a paucity of data regarding the hydraulic functions of coarse aggregates with intraparticle porous networks (Raviv et al., 2008b; Stovin et al., 2015), although data are emerging from a few nursery horticulture (Schindler et al., 2016) and green roof (Dal Ferro et al., 2014; Graceson et al., 2013a; Latshaw et al., 2009) research communities. Liu and Fassman-Beck (2017) are among the first to publish data on unsaturated flow and WRCs for engineered media for green roofs and bioretention soils. This study builds on this work and examines the properties of bulk mineral and biological green roof materials, including the WRCs, PSD, and hydrophobicity, and considers the implications for their use in extensive green roof systems up to 15 cm in depth.

Materials and Methods

Ten coarse soilless granular materials (Table 1) were selected for analysis and comparison: uniformly graded silica sand (Sample A, serving as a control), six bulk materials (Samples B–G), and three commercial blended products, designed for use on extensive green roofs (Samples H–J).

Bulk physical properties, water retention curves, OM, and hydrophobicity were determined for each sample. X-ray computed tomography was completed for Sample I only.

Bulk Physical Properties

Moisture content was determined by oven drying to constant weight mass at 85 ± 5°C and measuring the change in weight (Landva et al., 1983). This temperature was used to ensure no oxidation or charring of organic materials occurred (Landva et al., 1983). Solid particle densities (ρ_s) were calculated using gas pycnometry, determined with a stereopycnometer (Quantachrome) supplied with compressed air. Porosity (ϕ) was calculated from dried bulk (ρ_d) and particle solid densities (ρ_s):

$$\phi = 1 - \frac{\rho_d}{\rho_s} \quad [1]$$

The PSD was determined by sieve analysis on air-dried samples. Screen number and sizes were no. 3/8 in (9.51 mm), no. 6 (3.36 mm), no. 12 (1.7 mm), no. 16 (1.18 mm), no. 30 (0.60 mm), no. 50 (0.300 mm), and no. 104 (0.106 mm). The coefficients of uniformity (C_U) and curvature (C_C) were calculated to assess gradation quality as

$$C_U = \frac{d_{60}}{d_{10}} \quad [2]$$

$$C_C = \frac{(d_{30})^2}{d_{60} d_{10}} \quad [3]$$

where d_{60}, d_{30}, and d_{10} are the diameters of the percentage of particles passed at 10, 30, and 60%, respectively.

Organic matter (OM) content (%) was determined by loss on ignition (550°C, 2 h) using a muffle furnace (Matthiessen et al., 2005). X-ray computed tomography was performed on an individual fragment of lava rock and porous material recovered from Sample I using v|tome|x's CT system (GE Instruments). Resolution

Table 1. Identity and shared sources of 10 sample materials for analysis and comparison.

Sample	Product
A	graded silica sand
B	lightweight expanded aggregate (LEA)—Supplier 1
C	lightweight expanded aggregate (LEA)—Supplier 2
D	crushed brick
E	¼-in screened composted wood
F	bark fines
G	shredded pine
H	commercially blended biologically derived medium—Manufacturer A
I	commercially blended mineral based medium—Manufacturer A
J	commercially blended mineral based medium—Manufacturer B

was 16.77-μm voxels; geometric analyses (circularity and fractal dimension) were performed with FracLac for ImageJ (Karperien, 2013; Schneider et al., 2012).

Water Interaction Properties

Test material samples (250 cm^3), selected from well-mixed materials, were packed, with shaking by hand, into stainless steel rings (SZ 250, UMS GmbH; 5-cm height) for hydraulic conductivity and drying curve measurements. Saturated hydraulic conductivity was measured 10 times, in five repeats of two replicates, using a 1-cm constant head pressure and 1-s measurement intervals on a KSAT apparatus (UMS GmbH). Rates were normalized to 10°C by accounting for the temperature dependence of water viscosity. Drying curves were acquired on single samples saturated for 24 to 30 h using an automated evaporation method with a HYPROP instrument with integrated balance (UMS GmbH) (Bezerra-Coelho et al., 2018; Schindler et al., 2016). The resulting WRCs were fitted to a bimodal, constrained van Genuchten expression, with the addition of an adsorptive water retention function (S^{ad}), which forces the volumetric water content to 0 at pF 6.8 (= 618,758 kPa) (HYPROP-FIT code 1211; Peters and Durner [2015]). This extrapolation was selected because these materials experience evaporative drying beyond the irreducible saturation point. The volumetric water content (θ, v/v) at a capillary pressure head (h, cm H_2O) is calculated as a function of the saturated water content (θ_s) and the residual water saturation (θ_r), with the curve-fitting parameters corresponding to the air-entry pressure (α_i, 1/cm) and the unitless pore size distribution (n_i). The bimodal distribution is weighted in the first two terms with w_i:

$$\theta(h)=\frac{w_1\left(\theta_s-\theta_{ad}\right)}{\left[1+\left(\alpha_1 h\right)^{n_1}\right]^{1-1/n_1}}+\frac{w_2\left(\theta_s-\theta_{ad}\right)}{\left[1+\left(\alpha_2 h\right)^{n_2}\right]^{1-1/n_2}}+\theta_{ad}S^{ad} \quad [4]$$

Capillary pressure head is related to matric potential by

$$h=\frac{-\psi_m}{\rho_w g} \quad [5]$$

where ρ_w is the density of water (kg m^{-3}), and g is the gravitational constant (m s^{-2}).

Integrating Eq. [4] also permits comparison of the maximum theoretical water storage across depths i to j (S_{i-j}) of these systems at different design depths up to 15 cm:

$$S_{(i-j)}=\int_i^j\left\{\frac{w_1\left(\theta_s-\theta_{ad}\right)}{\left[1+\left(\alpha_1 h\right)^{n_1}\right]^{1-1/n_1}}+\frac{w_2\left(\theta_s-\theta_{ad}\right)}{\left[1+\left(\alpha_2 h\right)^{n_2}\right]^{1-1/n_2}}\right\}dh \quad [6]$$

The adsorption term S^{ad} in Eq. [4] does not contribute in these relatively high saturation conditions and has been omitted from Eq. [6] for simplicity. Horticulturally important parameters were also derived from the WRCs. The FAS in the material at 15 cm head (FAS_{15}) and the plant available water at 15 cm head (PAW_{15}), defined as the difference between the water held under static tension (container storage) and the permanent wilting point (ψ_m = −1.5 MPa = 15,296 cm) (Tolk, 2003), can be calculated from

$$FAS_{15}=\phi-\theta\left(h_{15}\right) \quad [7]$$

$$PAW_{15}=\theta\left(h_{15}\right)-\theta\left(h_{15,296}\right) \quad [8]$$

Because the evaporative drying occurred in the absence of a flowing liquid phase, the Young–Laplace equation was used to determine the distribution of pore radii within each material:

$$r=\frac{-2\gamma\cos\delta}{\psi_m} \quad [9]$$

This relates the emptying pore radius (r, m) to the matric potential (ψ_m, Pa) as a function of the interfacial tension between water and air in the pore spaces (γ, 0.072 N m^{-1} at 20°C) and the receding contact angle between the materials (δ, °). The assumption is made that if medium wetting is complete prior to the drying measurements, the receding contact angle of the water–particle interface is 0° (Dal Ferro et al., 2014; Ravi et al., 2015). It is also assumed that the Laplace–Young equation is valid across the entire saturation range, down to air-dry conditions. At very low moisture and very negative matric potential conditions, water adsorption to the green roof media may become significant, and pore sizes obtained from the drying curves in combination with Eq. [8] may differ from pore sizes measured with mercury porosimetry.

Air-dry moisture content and related experiments were conducted in a laboratory with normal indoor climate control (20–22°C, 11–29% relative humidity). Hydrophobicity was related to dynamic contact angle data measured on samples with an FTA200 goniometer (First Ten Angstroms). Five replicates were conducted on each material, using individual particles or peds taken from air-dried subsamples. Samples were placed on glass slides, and droplets of water (15 μL) were deposited from <1-cm height using a computer-controlled syringe pump. The bulk shrink/swell properties were determined by packing (with shaking) 300 cm^3 of test material into a glass cylinder. Water was added until no trapped air pockets were visible but only to the surface of the test material to prevent floating the dry particles. The samples were soaked for 24 h, and the depth of the material was read on the side of the cylinder to the nearest 5-cm^3 increment. The samples were then dried to constant weight, and the particles were allowed to settle by tapping the base of the cylinder by hand before assessing the final volume. Statistical comparisons, including ANOVA and r values, were calculated using NCSS 10 (NCSS, 2015) and regression trees using Orange Data Mining (Demšar et al., 2013). Statistical analyses were performed for bulk physical and water interaction parameters.

Results and Discussion

Bulk Physical Properties

There was a large variation in bulk density (ρ_b), particle density (ρ_s), and porosity (ϕ) between the tested material types (Table 2). The ρ_b and ρ_s of the mineral-based materials (sand [A], lightweight expanded aggregate [LEA; B and C], brick [D],

and the commercial blends [I and J]) were significantly higher ($\geq$0.7 g cm^{-3}) than those of the biologically derived media ($\leq$0.42 g cm^{-3}) (compost [E], bark [F], pine [G], and commercial blend [H]). The crushed brick (D) had a similar ρ_s to the sand, but the packing of the larger irregular fragments led to a lighter-weight bulk material with a higher ϕ. Material D had a ϕ of 0.58, which was similar to a crushed brick sample used in Graceson et al. (2013b) but coarser and with a higher ϕ than that used in the green roof study (ϕ = 0.47) by Molineux et al. (2009).

None of the bulk mineral products (Materials A–D) held any measurable water content after open storage in the laboratory for several weeks (air-dry θ), whereas the biologically derived products (E, F, and G) retained some moisture. The compost (E) had the highest volumetric water content (air-dry θ = 0.11) after this period of air-drying. The compost (E) and the blended product (H) contained almost 50% OM by weight, whereas the bark (F) and pine (G) were almost entirely decomposed and contained 97 and 87% OM, respectively. High OM was strongly and positively correlated with high porosity (r = 0.86), both of which are associated with particulate wood products (Shmulsky and Jones, 2011). Similarly, bark porosity has been reported at 0.86, various composted green waste materials have porosity >0.7, and wood fiber has porosity up to 0.95, depending on settling and compaction treatments (Raviv et al., 2008a).

Well-graded gravels have $C_U \geq 4$ and $1 \leq C_C \leq 3$, whereas well-graded sands have $C_U \geq 6$ (ASTM, 2011). Apart from the LEA (B) and the compost (E), all of the bulk products (A, C, D, F, G) were poorly graded, as reflected by low C_U; the brick (D) and compost (E) also had a low C_C. The blended commercial materials (H, I, and J) were all more well-graded (i.e., C_U >6), although Material H had a low C_C (<1).

Under unsaturated conditions, limited areas of contact between the large particles may reduce the hydraulic conductivity; because the intraparticle pores increase surface roughness, they influence the processes of film flow. This has been described as Regime III flow, where the contact area between particles, containing capillary water, is constrained by the proportion of non-pore surface on the individual fragments (Carminati et al., 2008). Figure 2 shows a single image slice from an X-ray scan of a typical particle taken from the largest fraction (passing the largest sieve) of Material I. Analysis of 849 slices through this same particle shows a low degree of circularity (0.40) but also a low mean fractal dimension of the surface (D = 1.1), which indicates that the surface has low roughness.

Although the particle has ~60% internal porosity, at the image resolution used, few of these pores appear to connect to the outside surface. Those that do may be dead-end pores rather than extensive networks with high connectivity, and fluid entry into such pores is not favored under the normal atmospheric pressure conditions encountered on green roofs (Hemmings et al., 2009).

Table 2. Density, porosity, and organic matter content of 10 porous test materials.

Sample	Bulk physical properties†			Air-dry θ	Organic matter	C_U‡	C_C§
	ρ_b	ρ_s	ϕ				
	— g cm^{-3} —				%		
Sand (A)	1.58	2.65¶	0.40	0	0	2.0	1.0
LEA# (B)	1.08	2.42	0.56	0	0	20	1.8
LEA (C)	0.77	2.31	0.67	0	0	1.7	1.0
Brick (D)	1.13	2.67	0.58	0	1	2.9	0.9
Compost (E)	0.42	1.81	0.77	0.11	48	6.3	0.9
Bark (F)	0.22	1.41	0.84	0.08	97	4.8	1.2
Pine (G)	0.24	1.35	0.83	0.05	87	5.0	1.1
Commercial blend (H)	0.39	1.87	0.79	0.03	47	6.7	0.9
Commercial blend (I)	0.91	2.16	0.58	0.01	7	23	1.9
Commercial blend (J)	1.07	2.41	0.56	0.01	5	14	1.9

† ρ_b, bulk density; ρ_s, particle density; ϕ, porosity.
‡ Coefficients of uniformity.
§ Coefficient of curvature.
¶ Value assumed (Zihms et al., 2013).
# Lightweight expanded aggregate.

Water Release Curves and Saturated Hydraulic Conductivity

Drying van Genuchten parameters for all materials were fitted to the WRC data per Eq. [4]. The raw data and the fitted WRCs are presented in Fig. 3, and equation parameters are defined in Table 3. The sand (A), LEA (C), compost (E), and pine (G) showed significant dominance of the primary weighted subfactor (w_1), indicating an essentially unimodal pore distribution, and little influence of any secondary or intraparticle porosity. The remaining bulk samples LEA (B), brick (D), and bark (F) and the commercial blended materials (H, I, and J) had a more even weighting between α_1 and α_2 (i.e., w_1 <0.9), indicating a significant influence of a secondary pore network. In all cases, the observed water content after air drying was lower than the irreducible water content values shown in Table 3, justifying the

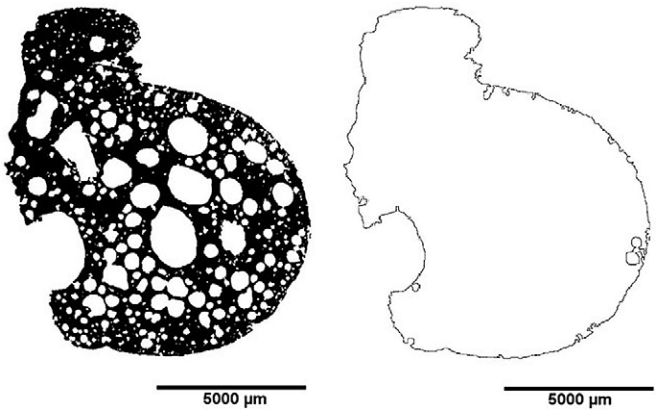

Fig. 2. Binary image from X-ray of Material I particle (left) and results of surface fractal analysis to show the network of pores (right).

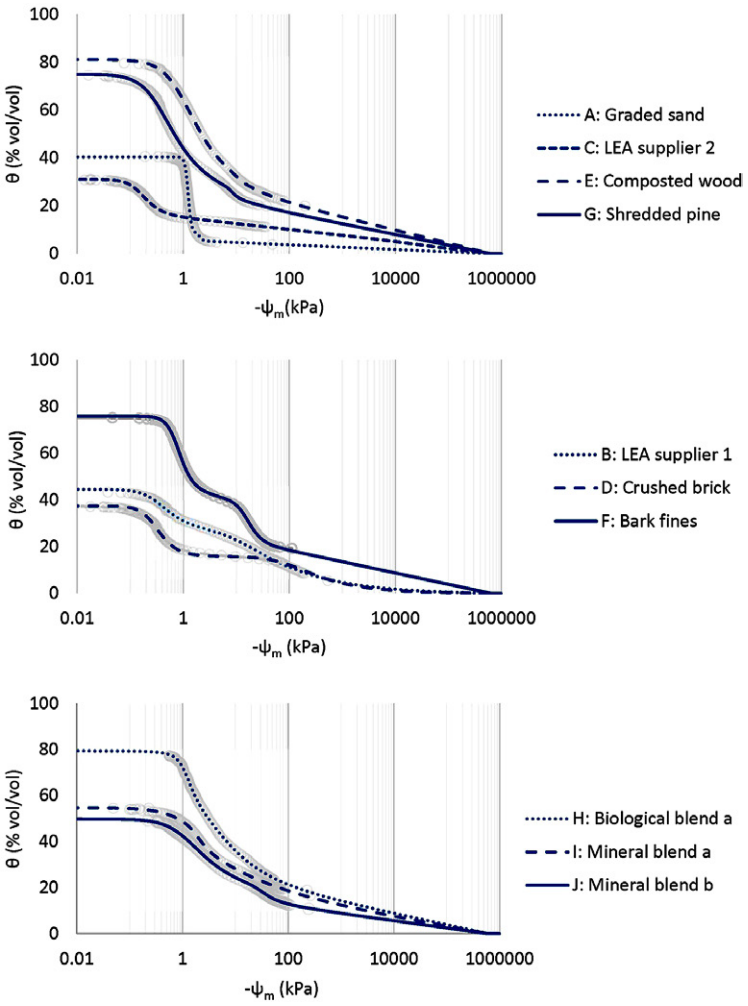

Fig. 3. Drying curve data from the analysis of 10 samples. Gray circles are raw data; lines are the fitted curves. Bulk materials A, C, E, and G are grouped as having significant (w_1 >0.9) weighting on the interparticle voids (top). Bulk materials B, D, and F are grouped as having distinctly separate and more evenly weighted van Genuchten parameters (middle). Blended materials (H, I, and J) are shown at the bottom. LEA, lightweight expanded aggregate.

Table 3. The van Genuchten parameters from the fitted curves arising from the evaporative drying of 10 test materials.

Sample	θ_r	θ_s	Interparticle voids			Intraparticle pores		
			w_1	α_1	n_1	w_2	α_2	n_2
	v/v			cm^{-1}			cm^{-1}	
Sand (A)	0.06	0.40	0.91	0.079	15	0.09	0.048	15
LEA† (B)	0.00	0.45	0.37	0.304	2.3	0.63	0.011	1.4
LEA (C)	0.16	0.31	0.93	0.650	3.1	0.07	0.000	1.3
Brick (D)	0.00	0.37	0.57	0.355	2.9	0.43	0.001	1.5
Compost (E)	0.32	0.81	0.97	0.118	1.9	0.03	0.010	7.7
Bark (F)	0.29	0.76	0.65	0.129	3.8	0.35	0.006	3.8
Pine (G)	0.28	0.75	0.94	0.300	1.9	0.06	0.012	7.8
Commercial blend (H)	0.28	0.79	0.34	0.080	4.5	0.66	0.041	1.7
Commercial blend (I)	0.23	0.55	0.78	0.110	1.4	0.22	0.053	4.4
Commercial blend (J)	0.18	0.50	0.85	0.098	1.7	0.15	0.003	3.8

† Lightweight expanded aggregate.

extrapolation into the adsorbed proportion of water in the samples under drier conditions.

The θ_s values were higher (≥0.75) in the biological samples than in the mineral samples (≤0.55), corresponding with the higher ϕ in the biological materials. For most samples, ϕ and θ_s values were similar, indicating little discrepancy between the measurement methods. Specifically, for A, E, and I, the difference between ϕ and θ_s was <0.05 $m^3\ m^{-3}$; for F, G, and J, this difference was between 0.05 and 0.1 $m^3\ m^{-3}$; and for B, this difference was between 0.1 and 0.2 $m^3\ m^{-3}$. For C and D, the differences were 0.36 and 0.21 $m^3\ m^{-3}$, respectively. These differences could have been related to pore spaces within the particles that were accessible by the compressed air during pycnometry but were not filled with water by soaking in the 5-cm-deep HYPROP apparatus. The physical characteristics of Material C are also evident in Fig. 2. The rapid drainage of the interparticle pores in this coarse, poorly graded, light-weight expanded aggregate is seen in the high α_1 value (0.650 cm^{-1}) related to low air-entry pressure. There is a very low weighting (w_2 = 0.07) of the secondary intraparticle pores in Material C. Expanded aggregates have been reported to have relatively little intraparticle porosity compared with other anthropogenic or naturally porous granular materials (Hemmings et al., 2009).

Figure 4 illustrates the narrow distribution of interparticle voids in the uniformly graded sand (A), corresponding with the high and matched n values of 15. This fits with the classical models relating PSD to pore size distributions and to matric potential. The WRC of the compost (E) demonstrated a very consistent drying rate (Fig. 3) that was dominated by a relatively narrow pore size distribution with a low n_1 (1.9), which matches the well-graded particle distribution seen in Fig. 4. Any intraparticle pore networks present are obscured by the fraction of finer fragments, which would also create smaller voids within the bulk matrix. The shredded pine (G) follows a similar trend, although an inflection in the curve suggests that there may be some influence of particularly small intraparticle pores at higher matric potential.

The bimodal distribution of pore networks in LEA (B), brick (D), and bark (F) manifest as even weightings between air entry pressures (α values) (Table 3). The bimodality is apparent as two peaks in the pore size distributions (Fig. 5). Naasz et al. (2008) has also described a largely bimodal pore distribution in pine bark with the following parameters: w_1 = 0.33, α_1 = 3.56 kPa^{-1}, and w_2 = 0.62, α_2 = 2.07 kPa^{-1}. Brick (Material D) had the smallest secondary pore network, centered around 0.8 μm, compared with Materials B (7 μm) and F (9 μm), whereas bark (F) had a notably narrower distribution of secondary pores (n_2 = 3.8) compared with the other two materials. The distinction of the smallest (in D) and comparatively regular pores (in F) can be distinguished qualitatively in Fig. 5.

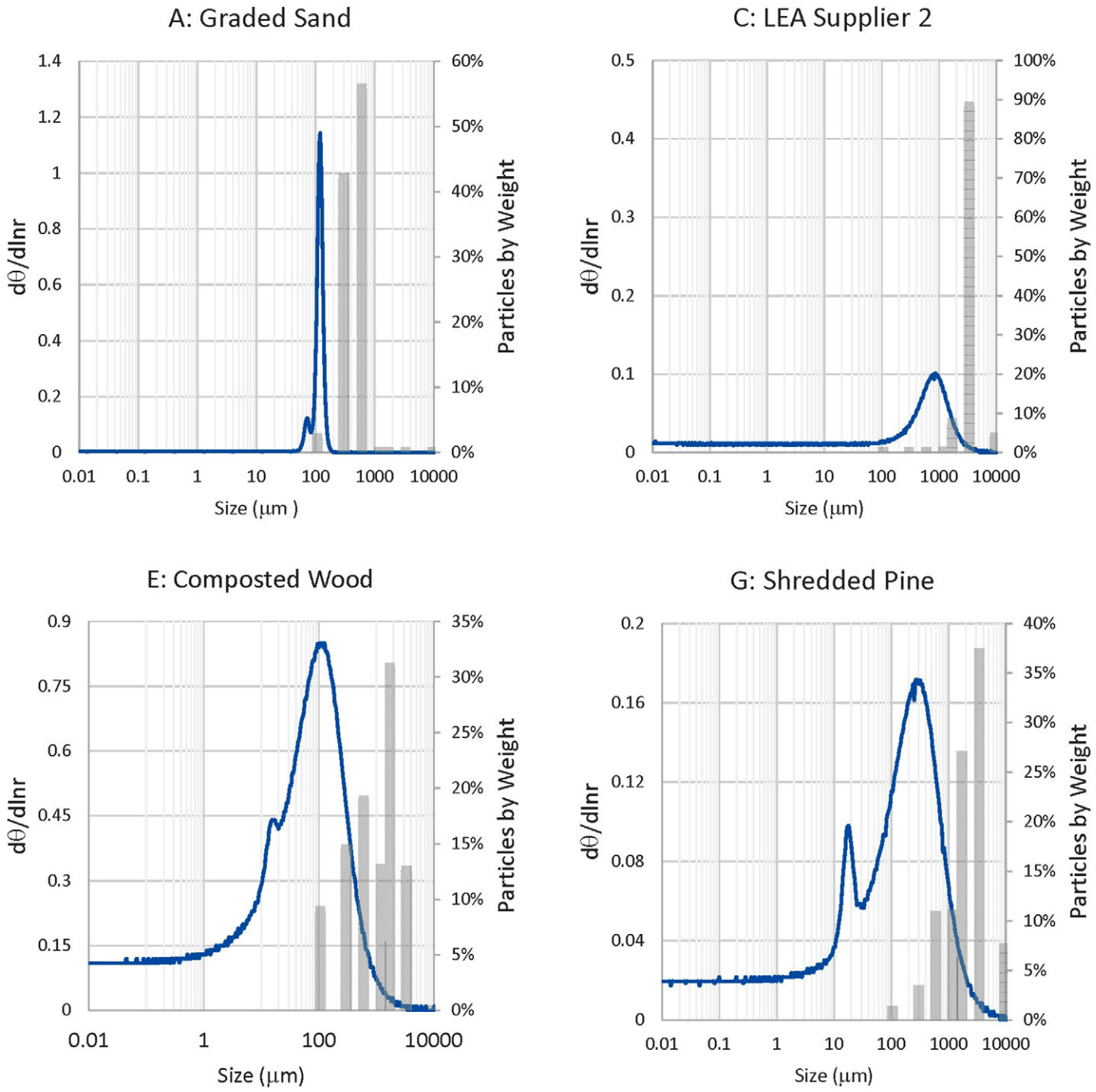

Fig. 4. The largely unimodal pore size distributions (line) plotted over the particle size distributions (bars) found in sand (A), poorly graded lightweight expanded aggregate (LEA) (C), 1/4-in screened composted wood (E), and shredded pine (G).

The LEA (B) in Fig. 5 was well-graded in comparison to LEA (C) from another supplier (Fig. 4). The secondary pore network in B may be due to smaller particles below those characterized by sieve analysis; this is suggested by a relatively high proportion of particles in the lowest fraction. Also, because B did not have the same discrepancy between ϕ and θ_s as found in C, the smaller spaces appear to be well connected as interparticle voids, preventing trapped air. Materials B and F were more well-graded than Material D (Fig. 5). However, none of these materials was significantly gap-graded (i.e., none was missing a mid-sized particle fraction), which could create a bimodal distribution of interparticle void sizes. Neither D nor F had pores visible to the naked eye within the particles; however, intraparticle pores with mode ~10 μm in both materials were visible under optical microscopy, as were those in Material B (Fig. 6).

The three commercial blended materials (H, I, and J) had balanced weightings between the two pore networks, as determined from air entry pressures (α values), which is indicative of these

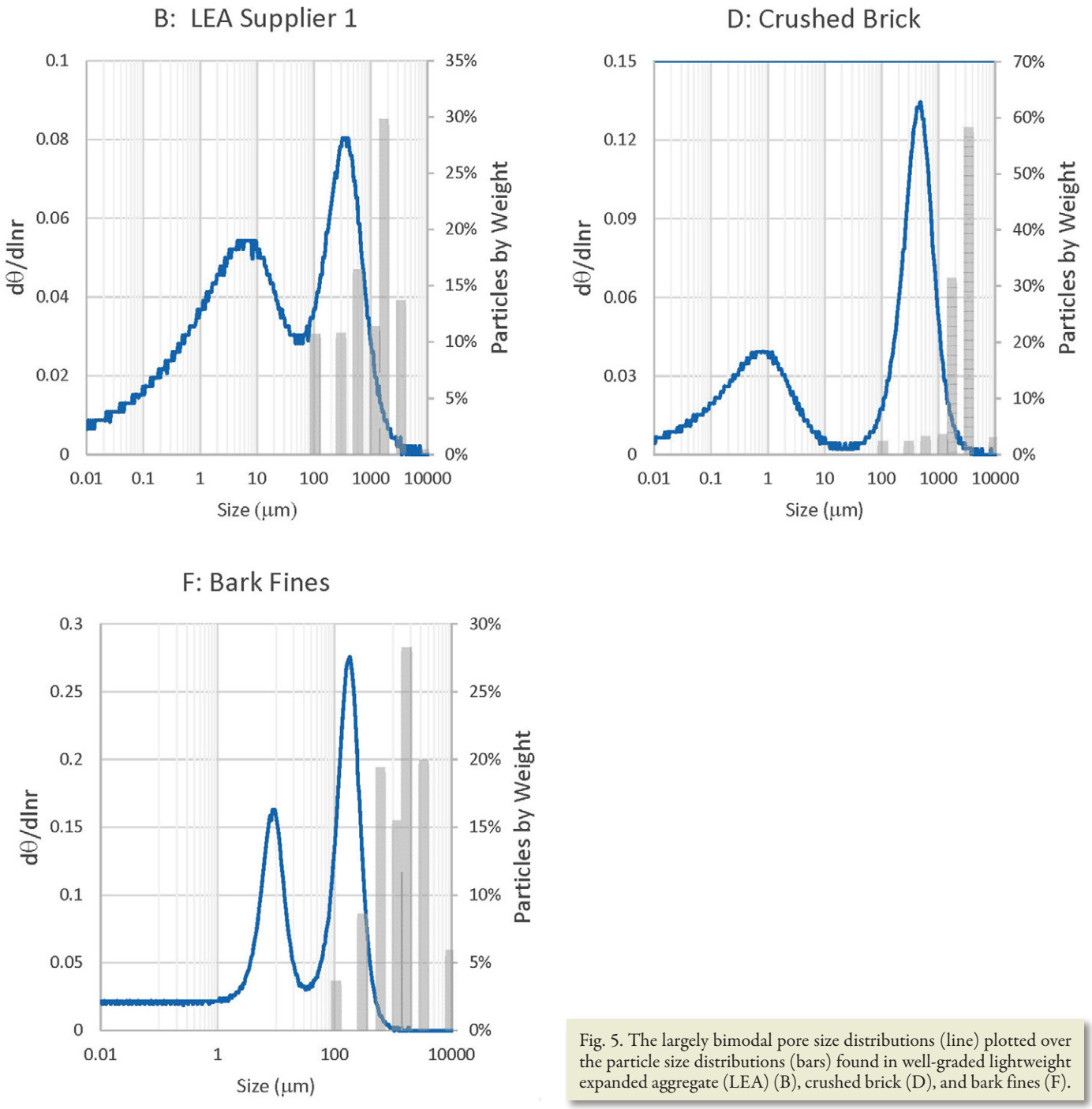

Fig. 5. The largely bimodal pore size distributions (line) plotted over the particle size distributions (bars) found in well-graded lightweight expanded aggregate (LEA) (B), crushed brick (D), and bark fines (F).

materials containing several constituents, such as expanded shale, brick fragments, and compost fines. Materials I and J had relatively low air entry pressure (i.e., high α_1 of 0.110 and 0.098 cm^{-1}) and contained correspondingly higher proportions of coarse fragments compared with the other the biologically derived mixture (H) (Fig. 7). The biologically derived commercial blend H was similarly graded and of similar appearance to the screened compost (E). Although H had a balanced weighting between two pore ranges ($w_2 = 0.66$) compared with E, these materials shared a wide pore size distribution and similar values for saturated water content θ_s and maximum adsorbed water content θ_r ($\sim$0.8 and 0.3, respectively). Because the α_1 value for Material H was of the same order of magnitude as α_2 (0.080 and 0.041 cm^{-1}), the pore distribution is not clearly separated into two distinct domains, as can be seen in the gradually changing slope of the curve in Fig. 7. As in Material B, there was a relatively high proportion of particles in the lowest fraction after sieve analysis of H, and there was no evidence of trapped air in comparison of ϕ and θ_s. These observations suggest again that a network of smaller interparticle voids, rather than intraparticle pores, are within the commercial blend H.

Table 4 presents the measured K_{sat} values and the calculated parameters of maximum system water storage (mm per 15 cm),

Fig. 6. Surface detail visible under 100× magnification (not to scale; image diameter is 1.7 mm): Material B (lightweight expanded aggregate) (left); Material D (brick particle) (center); Material F (bark fragment) (right).

$\theta(h_{15})$, $\theta(h_{15296})$, FAS_{15}, and PAW_{15}. The maximum water storage was correlated against the physical parameters of the media: d_{10}, ϕ, proportion of fines passing a no. 104 sieve, C_U, C_C, OM, α_1, and α_2. Higher storage was most strongly and negatively correlated with increasing size of the d_{10} fraction ($r = -0.86$) and positively correlated with the proportion of fines ($r = 0.52$). These relationships indicate the influence of the smallest interparticle voids by increasing the retention of capillary water at higher potential. A strong negative correlation between theoretical maximum water storage and α_1 ($r = -0.80$) confirms that the air entry pressure

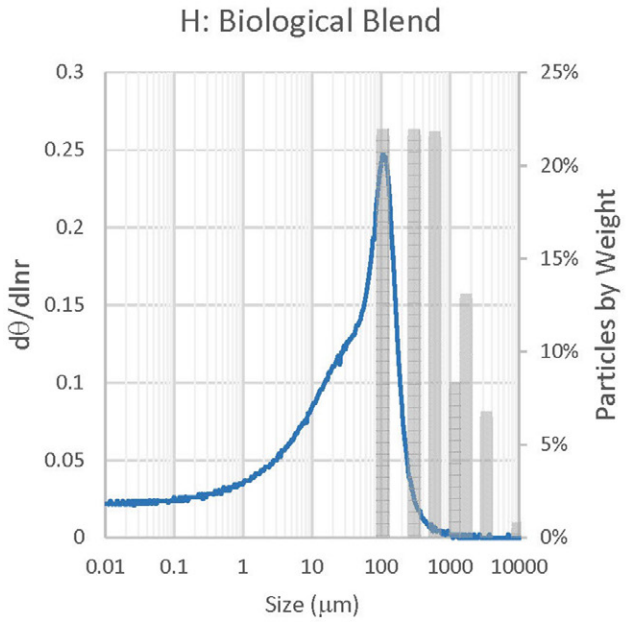

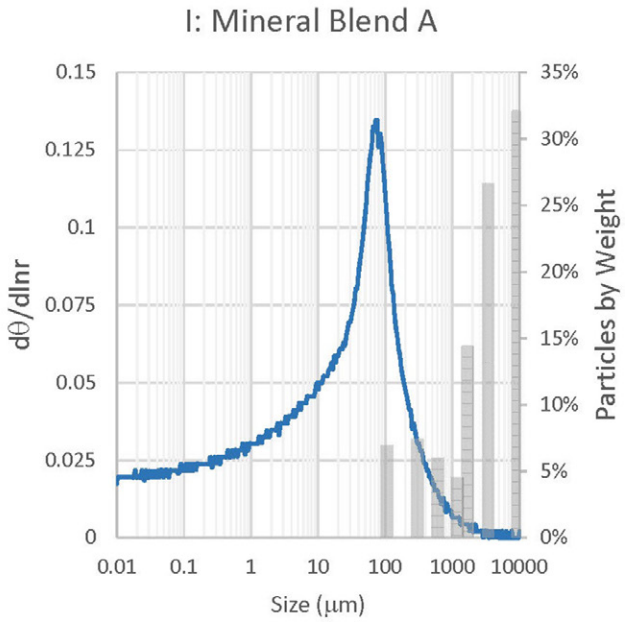

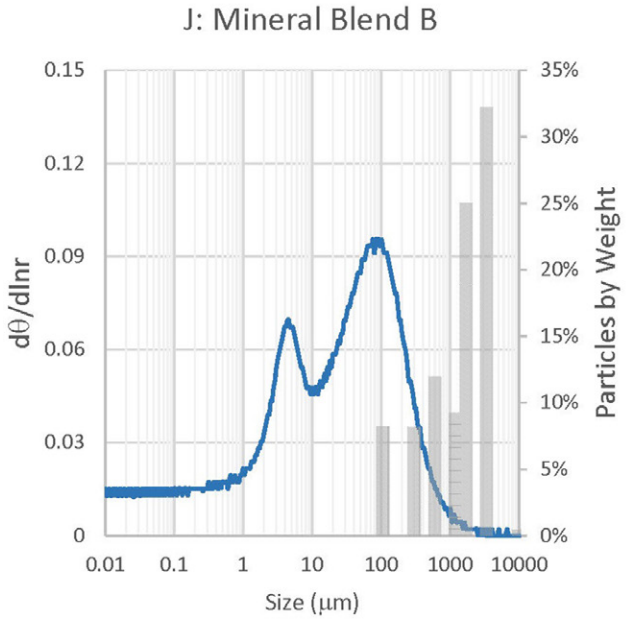

Fig. 7. Pore size distributions (line) plotted over particle size distributions (bars) found in commercial green roof planting media blends: Material H (compost based, Manufacturer A); Material I (mineral based, Manufacturer A); Material J (mineral based, Manufacturer B).

Table 4. System static and dynamic air and water properties for 10 samples

Sample	Properties†				
	K_{sat} (σ)	FAS_{15}	$\theta(h_{15})$	$\theta(h_{15296})$	PAW_{15}
	m h^{-1}	v/v			
Sand (A)	2.7 (0.6)	0.29	0.11	0.03	0.09
LEA‡ (B)	8.3 (6.3)	0.26	0.29	0.04	0.26
LEA (C)	13.6 (4.6)	0.52	0.15	0.07	0.08
Brick (D)	13.2 (3.9)	0.41	0.17	0.03	0.13
Compost (E)	1.6 (1.0)	0.20	0.57	0.14	0.43
Bark (F)	1.8 (1.4)	0.36	0.48	0.13	0.36
Pine (G)	8.3 (3.5)	0.43	0.39	0.12	0.28
Commercial blend (H)	0.9 (0.02)	0.15	0.64	0.13	0.50
Commercial blend (I)	0.4 (0.01)	0.13	0.45	0.13	0.34
Commercial blend (J)	0.3 (0.06)	0.17	0.39	0.08	0.31

† K_{sat}, saturated hydraulic conductivity; FAW_{15}, free air space in the material at 15 cm head; $\theta(h_{15})$, prediction of container storage; $\theta(h_{15296})$, prediction of wilting point.
‡ Lightweight expanded aggregate.

is also highly significant, controlling the onset of gravity water drainage under low tension. All the tested materials demonstrated acceptable (>10%) FAS in the upper part of the green roof profiles modeled (FAS_{15}). The compost (E) and the blended material (H) each provided the greatest PAW_{15} (0.43 and 0.50, respectively). The poorly graded sand (A) and LEA (C) provided almost no PAW_{15} (0.09 and 0.08, respectively).

In Fig. 8, a regression tree analysis was applied as a pedotransfer function to predict the $\theta(h_{15})$ and $\theta(h_{15296})$ values from the frequently tested parameters (ρ_d, ϕ, OM, C_U, C_C, d_{10}) and the proportion of fines (passing 100 μm). Organic matter was the primary predictor in each model and was associated with higher θ in both instances. Sandoval et al. (2017) similarly found that OM was strongly correlated with water retention capacity.

In the low-OM class (OM <3%), the water retention properties were controlled by the size of the smallest particles, with smaller fines increasing the water retained. In the higher-OM materials, which included all of the blends, higher water retention at 15 cm was associated with notably low C_C, which indicates both a higher proportion of fines and relatively few larger particles.

The material water capacity and K_{sat} were negatively correlated (−0.69). The K_{sat} values of Materials A through G have high SDs; the variation occurred between replicates rather than between repeated measurements, reflecting the heterogeneity of the materials rather than internal erosion processes (Chapuis, 2012). The commercial blended products (H, I, and J) had the lowest values of saturated hydraulic conductivity (each <0.5 m h^{-1}). The highest values were observed in the coarsest bulk materials (C and D each >13 m h^{-1}). Despite the use of a low and constant head pressure during the testing, the rapidity of flow in these materials was outside of the specifications of the K_{sat} instrument (i.e., >8.3 m h^{-1}). A higher K_{sat} value was associated with lower α_1 ($r = 0.92$) and larger d_{10} ($r = 0.79$).

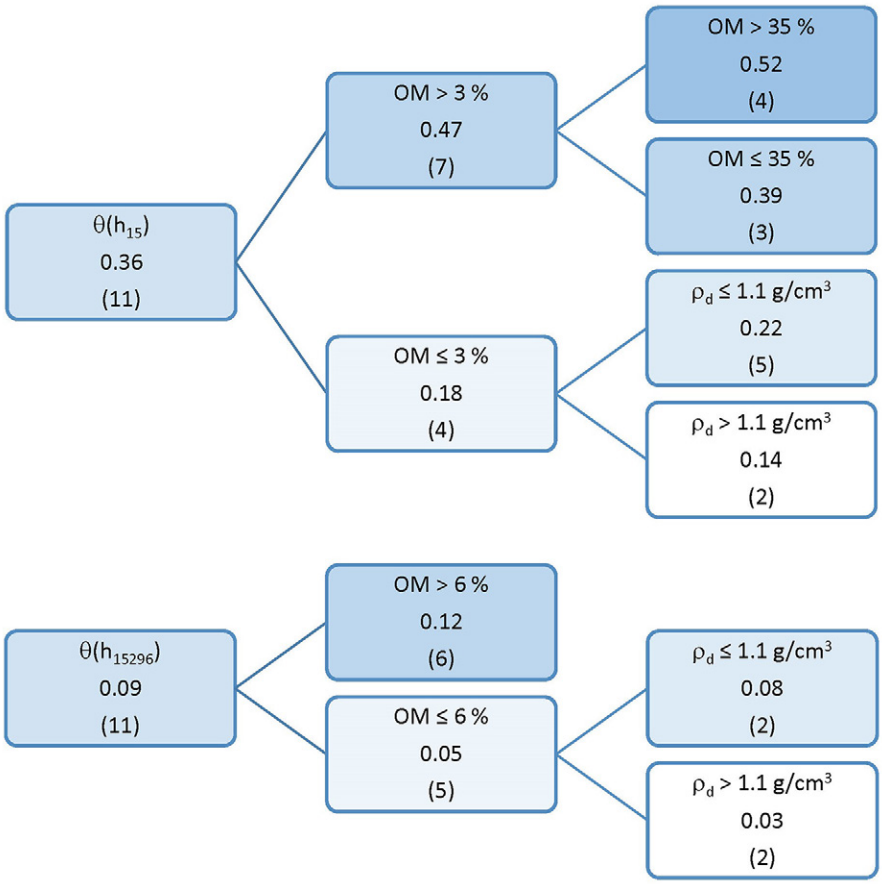

Fig. 8. Regression trees for prediction of container storage [$\theta(h_{15})$] and wilting point [$\theta(h_{15296})$] from predictors organic matter (OM), coefficient of curvature (C_C), diameter of the percentage of particles passed at 10% (d_{10}), and dried bulk density (ρ_d). The central figure in each node is the group mean. The number of cases is shown in parentheses. $\theta(h_{15})$, $R^2 = 0.965$; $\theta(h_{15296})$, $R^2 = 0.983$.

Hydrophobicity

The initial advancing contact angles ≥90° in Table 5 indicate that all three biologically derived bulk materials (E, F, and G) and the commercial blended material (H) were hydrophobic when air dry. The high SD of the measurements reflects the heterogeneity in the surface properties of the fragments at the scale of the testing. Rewetting of the fragments in compost (E) and bark (F) was relatively rapid, taking place in just 6 or 8 min, whereas the pine (G) and commercial blend (H) required over 20 min to rewet. The long rewetting time of Materials G and H could

Table 5. Dynamic contact angle data from the analysis of the biologically derived materials E, F, and G.

Sample	Mean initial contact angle (σ)	Mean wetting time (σ)	Depth after soaking	Depth after drying
	°	min	%	
Compost (E)	98 (7)	6 (6)	100	87
Bark (F)	90 (10)	8 (7)	102	87
Pine (G)	109 (10)	29 (7)	108	100
Commercial blend (H)	111 (8)	26 (4)	103	90

inhibit adsorption of draining water during more short, high-intensity rainstorms, particularly in summer months when the materials would be drier at onset. Dry bark has been reported as hydrophobic as a bulk characteristic (Beardsell and Nichols, 1982) and partially hydrophobic by static contact angle (60–80°) (Naasz et al., 2008). The initial contact angles measured in this study were at much higher tensions (~13 MPa) than those observed by Naasz et al. (2008) (up to ~0.3 MPa). Material G showed the greatest increase in volume through a single cycle of wetting and drying; the other three materials settled further.

Conclusions

Although some of these coarse materials (e.g., the lightweight expanded aggregate, crushed brick, and bark fines) contain measurable intraparticle porosity, the impact of these networks on bulk material properties is minimal. The poorly graded bulk materials (A–G) demonstrated high mean K_{sat}, with larger variability, compared with the <1 m h^{-1} observed in all three commercially blended products (H, I, and J). Across the whole data set, K_{sat} is correlated to the d_{10}, which is in agreement with many observations and calculations made in natural soils (Chapuis, 2012). The pores observed in some particles may influence hydraulic conductivity under drier conditions by increasing surface roughness and reducing the area of contact between adjacent fragments.

The fitted WRCs indicated that both the largest and finest interparticle void spaces were influential in determining the water capacity of the materials. Overall, the commercial blended products maintained a higher proportion of their retention per unit depth compared with the bulk materials. Because the coarse bulk materials had low air entry pressures (i.e., large van Genuchten α values), the water retention of many of these materials dropped significantly within the upper parts of the 15-cm maximum specification for extensive green roofs. The implication is that the addition of a few extra centimeters of planting material is not necessarily the most effective way to increase the storm water capture of an extensive system. Instead, design specifications should focus on using a well-graded medium with a high capacity for capillary retention of water allowing greater storage of the green roof system. Higher water retention in the upper portion of a green roof may also increase the evaporation potential of a green roof.

When used in green roof applications, the drainage of the materials will also depend heavily on the properties of the lower seepage face boundary (geotextile). To make properly informed design decisions, this factor warrants further exploration.

Acknowledgments

We thank the Miller Group and Gro-Bark for providing sample materials used in this study and Flynn Canada Ltd. for their financial contribution to an Industrial Postgraduate Scholarship with the Natural Sciences and Engineering Research Council of Canada (NSERC) to support this research. None of the parties listed above contributed to data interpretation, article writing, or publication decisions.

References

Adams, B.J., and F. Papa. 2000. Urban stormwater management planning with analytical probabilistic models. John Wiley & Sons, Hoboken, NJ.

ASTM. 2011. D2487-11: Standard practice for classification of soils for engineering purposes (Unified Soil Classification System). ASTM Int., West Conshohocken, PA. doi:10.1520/D2487-11

Babilis, D.J., and P.A. Londra. 2011. Assessment of various methods for the determination of hydraulic conductivities of two green roof substrates by steady state infiltration experiments. Irrig. Drain. 60:274–280. doi:10.1002/ird.543

Beardsell, D.V., and D.G. Nichols. 1982. Wetting properties of dried-out nursery container media. Sci. Hortic. 17:49–59. doi:10.1016/0304-4238(82)90061-9

Bezerra-Coelho, C.R., L. Zhuang, M.C. Barbosa, and M.Th. van Genuchten. 2018. Further tests of the HYPROP evaporation method for estimating the unsaturated soil hydraulic properties. J. Hydrol. Hydromech. 66:161–169. doi:10.1515/johh-2017-0046

Breuning, J. 2013. Irrigation on extensive green roofs: Facts study. Green Roof Serv., Baltimore, MD. http://www.greenrooftechnology.com/_literature_174681/Irrigation_and_Extensive_Green_Roofs (accessed 15 Apr. 2019).

Bursztа-Adamiak, E. 2012. Analysis of the retention capacity of green roofs. J. Water Land Dev. 16:3–9. doi:10.2478/v10025-012-0018-8

Carbone, M., G. Garofalo, G. Nigro, and P. Piro. 2014. A conceptual model for predicting hydraulic behaviour of a green roof. Procedia Eng. 70:266–274. doi:10.1016/j.proeng.2014.02.030

Carminati, A., A. Kaestner, P. Lehmann, and H. Flühler. 2008. Unsaturated water flow across soil aggregate contacts. Adv. Water Resour. 31:1221–1232. doi:10.1016/j.advwatres.2008.01.008

Carter, T., and C.R. Jackson. 2007. Vegetated roofs for stormwater management at multiple spatial scales. Landsc. Urban Plan. 80:84–94. doi:10.1016/j.landurbplan.2006.06.005

Carter, T.L., and T.C. Rasmussen. 2006. Hydrologic behaviour of vegetated roofs. J. Am. Water Resour. Assoc. 42:1261–1274. doi:10.1111/j.1752-1688.2006.tb05611.x

Cassel, D.K., and D.R. Neilsen. 1986. Field capacity and available water capacity. In: A. Klute, editor, Methods of soil analysis. Part 1. Physical and mineralogical methods. 2nd ed. SSSA Book Ser. 5. SSSA and ASA, Madison, WI. p. 901–924. doi:10.2136/sssabookser5.1.2ed.c36

Chapuis, R. 2012. Predicting the saturated hydraulic conductivity of soils: A review. Bull. Eng. Geol. Environ. 71:401–434. doi:10.1007/s10064-012-0418-7

Cronk, E. 2012. Stormwater retention capabilities of steep sloped, extensive green roof systems. M.A. thesis. Univ. of Michigan, East Lansing.

Czemiel Berndtsson, J. 2010. Green roof performance towards management of runoff water quantity and quality: A review. Ecol. Eng. 36:351–360. doi:10.1016/j.ecoleng.2009.12.014

Dal Ferro, N., C. Pagliarin, and F. Morari. 2014. Pore network and water retention characteristics of volcanic porous media. Eur. J. Soil Sci. 65:672–683. doi:10.1111/ejss.12163

Demšar, J., T. Curk, A. Erjavec, Č. Gorup, T. Hočevar, M. Milutinovič, et al. 2013. Orange: data mining toolbox in Python. J. Mach. Learn. Res. 14:2349–2353.

Fassman-Beck, E., W. Hunt, R. Berghage, D. Carpenter, T. Kurtz, V. Stovin, and B. Wadzuk. 2016. Curve number and runoff coefficients for extensive living roofs. J. Hydrol. Eng. 21(3):04015073. doi:10.1061/(ASCE)HE.1943-5584.0001318

Forschungsgesellschaft Landschaftsentwicklung–Landschaftsbau. 2008. Guidelines for the planning, construction and maintenance of green roofing: Green roofing guideline. Forschungsgesellschaft Landschaftsentwicklung–Landschaftsbau, Bonn.

Graceson, A., M. Hare, J. Monaghan, and N. Hall. 2013a. The water retention capabilities of growing media for green roofs. Ecol. Eng. 61:328–334. doi:10.1016/j.ecoleng.2013.09.030

Graceson, A., M. Hare, J. Monaghan, and N. Hall. 2013b. The water retention capabilities of growing media for green roofs. Ecol. Eng. 61:328–334. doi:10.1016/j.ecoleng.2013.09.030

Gregoire, B.G., and J.C. Clausen. 2011. Effect of a modular extensive green roof on stormwater runoff and water quality. Ecol. Eng. 37(6):963–969. doi:10.1016/j.ecoleng.2011.02.004

Handreck, K.A., and N.D. Black. 2002. Growing media for ornamental plants and turf. UNSW Press, Kensington, NSW, Australia.

Hathaway, A.M., W.F. Hunt, and G.D. Jennings. 2008. A field study of green roof hydrologic and water quality performance. Trans. ASABE 51:37–44. doi:10.13031/2013.24225

Heller, H., A. Bar-Tal, S. Assouline, K. Narkis, S. Suryano, A. de la Forge, et al. 2015. The effects of container geometry on water and heat regimes in soilless culture: Lettuce as a case study. Irrig. Sci. 33:53–65. doi:10.1007/s00271-014-0448-y

Hemmings, R.T., B.J. Cornelius, P. Yuran, and M. Wu. 2009. Comparative study of lightweight aggregates. Paper presented at: World of Coal Ash (WOCA) Conference, Lexington, KY. 4–7 May 2009.

Hill, J., J. Drake, and B. Sleep. 2016. Comparisons of extensive green roof media in southern Ontario. Ecol. Eng. 94:418–426. doi:10.1016/j.ecoleng.2016.05.045

Hill, J., A.P.J. Drake, B. Sleep, and L. Margolis. 2017. Influences of four extensive green roof design variables on stormwater hydrology. J. Hydrol. Eng. doi:10.1061/(ASCE)HE.1943-5584.0001534

Hill, J., H. Kuszkowski, B. Sleep, and J. Drake. 2015. Gone with the wind? In: Environmental Connection Conference: Proceedings of a meeting held in Portland, OR. 16–18 Feb. 2015. Int. Erosion Control Assoc., Aurora, CO.

Hilten, R.N., T.M. Lawrence, and E.W. Tollner. 2008. Modeling stormwater runoff from green roofs with HYDRUS-1D. J. Hydrol. 358:288–293. doi:10.1016/j.jhydrol.2008.06.010

Iwata, S., T. Tabuchi, and B.P. Warkentin. 1994. Capillarity. In: Soil-water interactions: Mechanisms applications. 2nd ed. CRC Press, Boca Raton, FL. p. 229–256.

Karperien, A. 2013. FracLac for ImageJ: User's guide. Natl. Inst. Health, Bethesda, MD. http://rsb.info.nih.gov/ij/plugins/fraclac/FLHelp/Introduction.htm (accessed 1 June 2016).

Kasmin, H., V.R. Stovin, and E.A. Hathway. 2010. Towards a generic rainfall–runoff model for green roofs. Water Sci. Technol. 62:898–905. doi:10.2166/wst.2010.352

Khoshand, A., and M. Fall. 2014. Geotechnical characterization of compost based biocover materials. Geotech. Geol. Eng. 32:489–503. doi:10.1007/s10706-014-9728-9

Landva, A., E. Korpijaakko, and P. Pheeney. 1983. Geotechnical classification of peats and organic soils. In: P.M. Jarrett, editor, Testing of peats and organic soils. ASTM Int., West Conshohocken, PA. p. 37–115.

Latshaw, K., J. Fitzgerald, and R. Sutton. 2009. Analysis of green roof growing media porosity. RURALS: Rev. Undergrad. Res. Agric. Life Sci. 4(1):2.

Li, Y., and R.W. Babcock. 2014. Green roof hydrologic performance and modeling: A review. Water Sci. Technol. 69:727–738. doi:10.2166/wst.2013.770

Liu, R., and E. Fassman-Beck. 2017. Port structure and unsaturated hydraulic conductivity of engineered media for living roofs and bioretention based on water retention data. J. Hydrol. Eng. 23(3):04017065. doi:10.1061/(ASCE)HE.1943-5584.0001621

Ma, L., B. Qin, and Q.Z. Chang. 2012. Performance of urban rainwater retention by green roof: A case study of Jinan. Appl. Mech. Mater. 178–181:295. doi:10.4028/www.scientific.net/AMM.178-181.295

MacIvor, J.S., L. Margolis, C.L. Puncher, B. Carver, and J. Matthews. 2013. Decoupling factors affecting plant diversity and cover on extensive green roofs. J. Environ. Manage. 130:297–305. doi:10.1016/j.jenvman.2013.09.014

Matthiessen, M.K., F.J. Larney, L. Brent Selinger, and A.F. Olson. 2005. Influence of loss-on-ignition temperature and heating time on ash content of compost and manure. Commun. Soil Sci. Plant Anal. 36:2561–2573. doi:10.1080/00103620500257242

McCoy, E. 2014. Drainage systems for golf courses. Ohio State Univ., Columbus. https://kb.osu.edu/bitstream/handle/1811/65469/2/SENR_mccoy_golf_courses_DrainageSystems.pdf (accessed 15 Apr. 2019).

McGlade, T., and J. Hill. 2014. Success and succession. Presented at: Cities alive: 12th Annual Green Roof and Wall Conference, Nashville, TN. 12–15 Nov. 2004.

Metselaar, K. 2012. Water retention and evapotranspiration of green roofs and possible natural vegetation types. Resour. Conserv. Recycl. 64:49–55. doi:10.1016/j.resconrec.2011.12.009

Molineux, C.J., C.H. Fentiman, and A.C. Gange. 2009. Characterising alternative recycled waste materials for use as green roof growing media in the U.K. Ecol. Eng. 35:1507–1513. doi:10.1016/j.ecoleng.2009.06.010

Naasz, R., J.-C.C.-C. Michel, and S. Charpentier. 2008. Water repellency of organic growing media related to hysteretic water retention properties. Eur. J. Soil Sci. 59:156–165. doi:10.1111/j.1365-2389.2007.00966.x

Nawaz, R., A. McDonald, and S. Postoyko. 2015. Hydrological performance of a full-scale extensive green roof located in a temperate climate. Ecol. Eng. 82:66–80. doi:10.1016/j.ecoleng.2014.11.061

NCSS. 2015. NCSS 10 statistical software. NCSS, Kaysville, UT.

Nelson, M.S., and T.M. Rittenour. 2015. Using grain-size characteristics to model soil water content: Application to dose-rate calculation for luminescence dating. Radiat. Meas. 81:142–149. doi:10.1016/j.radmeas.2015.02.016

Optigrün International. 2008. Green roof systems with granular drainage. Conservation Technol., Baltimore, MD. http://www.conservationtechnology.com/greenroof_systems_granular.html (accessed 8 May 2016).

Pachepsky, Y., and W.J. Rawls. 2004. Development of pedotransfer functions in soil hydrology. Elsevier, New York.

Palla, A., I. Gnecco, and L.G. Lanza. 2009. Unsaturated 2D modelling of subsurface water flow in the coarse-grained porous matrix of a green roof. J. Hydrol. 379:193–204. doi:10.1016/j.jhydrol.2009.10.008

Peters, A., and W. Durner. 2015. SHYPFIT 2.0 user's manual. Inst. Ökologie, Technische Univ., Berlin.

Petrell, R., and A. Gumulia. 2013. Saturated and unsaturated flow through sloped compost filter beds of different particle sizes. Water Sci. Technol. 67:2406–2411. doi:10.2166/wst.2013.108

Poë, S., V. Stovin, and C. Berretta. 2015. Parameters influencing the regeneration of a green roof's retention capacity via evapotranspiration. J. Hydrol. 523:356–367. doi:10.1016/j.jhydrol.2015.02.002

Poë, S., V. Stovin, and Z. Dunsiger. 2011. The impact of green roof configuration on hydrological performance. Presented at: 12th International Conference on Urban Drainage, Porto Alegre, Brazil. 11–16 Sept. 2011. IWA, London.

Prowell, E.S. 2006. An analysis of stormwater retention and detention of modular green roof blocks. M.S. thesis. Univ. of Georgia, Athens.

Qin, X., X. Wu, Y.-M. Chiew, and Y. Li. 2012. A green roof test bed for stormwater management and reduction of urban heat island effect in Singapore. Br. J. Environ. Clim. Change 2:410–420.

Ravi, S., R. Dharmarajan, and S. Moghaddam. 2015. Measurement of capillary radius and contact angle within porous media. Langmuir 31:12954–12959. doi:10.1021/acs.langmuir.5b03113

Raviv, M., J.H. Lieth. M. Maher, M. Prasad, and M. Raviv. 2008a. Soilless culture. Elsevier, New York.

Raviv, M., J.H. Lieth, and R. Wallach. 2008b. Soilless culture. Elsevier, New York.

Roofmeadow. 2013. Type III green roofs. Roofmeadow, Philadelphia, PA. http://www.roofmeadow.com/details-specs-services/details-specs/type-iii/ (accessed 8 May 2016).

Rossman, L., and W. Huber. 2015. Storm water management model reference manual. Vol. I. Hydrology. USEPA Office of Research and Development, Washington, DC.

Rowe, D.B., M.R. Kolp, S.E. Greer, and K.L. Getter. 2014. Comparison of irrigation efficiency and plant health of overhead, drip, and sub-irrigation for extensive green roofs. Ecol. Eng. 64:306–313. doi:10.1016/j.ecoleng.2013.12.052

Salarashayeri, A.F., and M. Siosemarde. 2012. Prediction of soil hydraulic conductivity from particle-size distribution. Int. J. Geol. Environ. Eng. 6:16–20.

Sandoval, V., C.A. Bonilla, J. Gironás, S. Vera, F. Victorero, W. Bustamante, et al. 2017. Porous media characterization to simulate water and heat transport through green roof substrates. Vadose Zone J. 16(4). doi:10.2136/vzj2016.10.0101

Schindler, U., L. Müller, and F. Eulenstein. 2016. Measurement and evaluation of the hydraulic properties of horticultural substrates. Arch. Agron. Soil Sci. 62:806–818. doi:10.1080/03650340.2015.1083982

Schneider, C.A., W.S. Rasband, and K.W. Eliceiri. 2012. NIH Image to ImageJ: 25 years of image analysis. Nat. Methods 9:671–675. doi:10.1038/nmeth.2089

Schroll, E., J. Lambrinos, T. Righetti, and D. Sandrock. 2011. The role of vegetation in regulating stormwater runoff from green roofs in a winter rainfall climate. Ecol. Eng. 37:595–600. doi:10.1016/j.ecoleng.2010.12.020

She, N., and J. Pang. 2010. Physically based green roof model. J. Hydrol. Eng. 15(6):458–464. doi:10.1061/(ASCE)HE.1943-5584.0000138

Shmulsky, R., and P.D. Jones. 2011. Density and specific gravity. In: Forest products and wood science: An introduction. Wiley-Blackwell, New York. p. 175–195.

Stovin, V., G. Vesuviano, and S. De-Ville. 2015. Defining green roof detention performance. Urban Water J. 14:574–588. doi:10.1080/1573062X.2015.1049279

Tolk, J.A. 2003. Soils, permanent wilting points. In: B.A. Stewart and T.A. Howell, editors, Encyclopedia of water science. Marcel Dekker, New York. p. 927–929.

Uhl, M., and L. Schiedt. 2008. Green roof storm water retention-monitoring results. Presented at: 11th International Conference on Urban Drainage, Edinburgh, UK. 31 Aug.–5 Sept. 2008.

van Genuchten, M.Th., F.J. Leij, and S.R. Yates. 1991. The RETC code for quantifying the hydraulic functions of unsaturated soils, version 1.0. USEPA, Ada, OK.

Van Seters, T., L. Rocha, D. Smith, and G. MacMillan. 2009. Evaluation of green roofs for runoff retention, runoff quality, and leachability. Water Qual. Res. J. Can. 44:33–47. doi:10.2166/wqrj.2009.005

VanWoert, N.D., D.B. Rowe, J.A. Andresen, C.L. Rugh, R.T. Fernandez, and L. Xiao. 2005. Green roof stormwater retention: effects of roof surface, slope, and media depth. J. Environ. Qual. 34:1036–1044. doi:10.2134/jeq2004.0364

Voyde, E., E. Fassman, and R. Simcock. 2010. Hydrology of an extensive living roof under sub-tropical climate conditions in Auckland, New Zealand. J. Hydrol. 394:384–395. doi:10.1016/j.jhydrol.2010.09.013

Wang, Y., S.M. Grove, and M.G. Anderson. 2008. A physical–chemical model for the static water retention characteristic of unsaturated porous media. Adv. Water Resour. 31:701–713. doi:10.1016/j.advwatres.2008.01.005

Yocca, D., and L.V. Sale. 2012. Green roof and wall performance standards. Living Archit. Monit. 14(1):16–17.

Yuristy, G. 2013. Considering a green roof substrate for northern climates. M.S. thesis. Univ. of Guelph, Guelph, ON, Canada.

Zhang, S., and Y. Guo. 2012. Analytical probabilistic model for evaluating the hydrologic performance of green roofs. J. Hydrol. Eng. 8:19–28.

Zihms, S., C. Switzer, J. Irvine, and M. Karstunen. 2013. Effects of high temperature processes on physical properties of silica sand. Eng. Geol. 164:139–145.